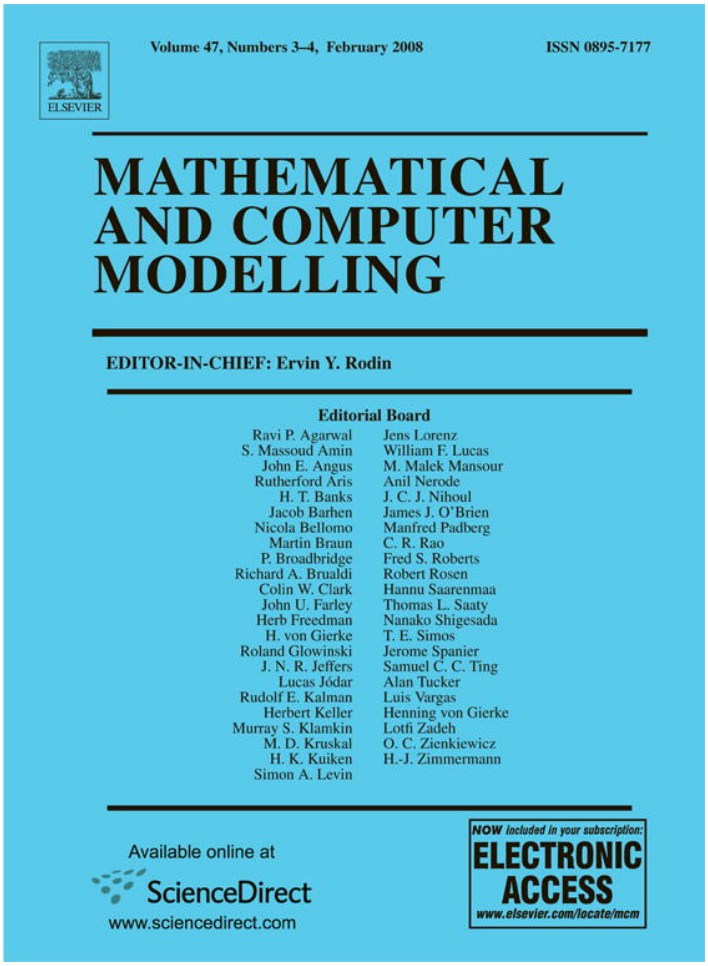

Available online at www.sciencedirect.com
ScienceDirect
Mathematical and Computer Modelling 47 (2008) 495–514
MATHEMATICAL AND COMPUTER MODELLING
www.elsevier.com/locate/mcm

Linear transport equations in flatland with small angular diffusion and their finite element approximations

M. Asadzadeh[a,b,*], E.W. Larsen[c]

[a] *Department of Mathematics, Chalmers University of Technology, SE-412 96 Goteborg, Sweden*
[b] *Department of Mathematics, 310 Malott Hall, Cornell University, Ithaca, NY 14853, USA*
[c] *Department of Nuclear Engineering and Radiological Sciences, University of Michigan, Ann Arbor, MI 48109, USA*

Received 12 April 2007; accepted 11 May 2007

Abstract

We study the flatland (two dimensional) linear transport equation, under an *angular* 2π *periodicity* assumption both on particle density function $\psi(x, y, \theta)$ and on the differential scattering $\sigma_s(\theta)$. We consider the beam problem, with a forward peaked source on phase-space, and derive P_1 approximation with a diffusion coefficient of $1/2\sigma_{\text{tr}}$, (versus $1/3\sigma_{\text{tr}}$ of the three dimensional problem), where σ_{tr} is the transport cross section. Further assumptions as peaked $\sigma_s(\theta)$ near $\theta = 0$ (*small angle of scattering*), and *small angle of flight* ($\theta \approx 0$) yield Fokker–Planck and Fermi approximations with the diffusion coefficients σ_{tr} (rather than $\sigma_{\text{tr}}/2$ of the three dimensional case). We discretize the problem using four different Galerkin schemes and justify the results through some numerical examples.

Keywords: Linear transport equation; Flatland; Fokker–Planck; Fermi; Standard Galerkin; Characteristic method; Streamline- and semi streamline diffusion methods

1. Introduction

This note is devoted to the study of the linear *flatland* transport equation with 2π periodic *probability density function* ψ and *differential scattering kernel* σ_s:

$$\begin{cases} \psi(x, y, \theta), & (x, y) \in \mathbb{R}^2,\ 0 \le \theta \le 2\pi, \\ \psi(\theta) = \psi(\theta + 2\pi), & \sigma_s(\theta) = \sigma_s(\theta + 2\pi), \end{cases} \tag{1.1}$$

$\psi \equiv \psi(x, y, \theta)$ is the number of particles in $\mathrm{d}x$ about x, $\mathrm{d}y$ about y and $\mathrm{d}\theta$ about θ.

Our objective is to derive the (angular) diffusion approximations for the linear Boltzmann equation in the flatland (2D with certain assumptions) case, construct some discrete computational algorithms and justify their efficiency and reliability through implementing some numerical examples. For the beam problem in the flatland case, and under the same assumptions as in the three dimensional case, we obtain P_1, *Fokker–Planck* and *Fermi* approximations with

* Corresponding address: Mathematics Department, Chalmers University of Technology, Goteborg University, SE-412 96 Goteborg, Sweden. Fax: +49 31 16 1973.
E-mail addresses: mohammad@math.chalmers.se (M. Asadzadeh), edlarsen@umich.edu (E.W. Larsen).

0895-7177/$ - see front matter
doi:10.1016/j.mcm.2007.05.004

diffusion coefficients different from those in the three dimensional case derived in, e.g., [1] and [2]. We present a formal approach reducing the 3D transport equation to the "flatland" transport equation. Starting from the "flatland" transport equation we derive the *usual balance equation* and a variational form underlying derivation of a beam problem as well as Fokker–Planck and Fermi developments. For other kinds of diffusion approximation for transport processes see, e.g. [3]. Finally we reformulate the equation as a model problem in a bounded domain associated with homogeneous mixed inflow boundary conditions, and product of Dirac δ functions as the *incident data*. The model problem is then discretized by means of four different Galerkin schemes: *Standard Galerkin* (SG), *Semi Streamline Diffusion* (SSD), *Characteristic Galerkin* (CG) and *Characteristic Streamline Diffusion* (CSD) methods. We implement these schemes in some numerical examples and justify the convergence in various norms as well as the impact of a modified L_2 projection, introduced e.g. in [4], in improving the qualitative behavior of the schemes regarding both formation of boundary layers and also the oscillatory behavior due to non-smooth data.

The "flatland" type transport equations are considered, e.g., in modelling the wave scattering in the marginal ice zone [5], where the ice floes have a small relative stiffness: ice floes tend to form with thicknesses of ~ 1 m and of a size of $\sim$100 m (1/2 or 1/4 of wavelengths). The corresponding, large scale, equations (for energy, *not* displacement) are governed by scattering theory. There are two approaches to scattering theory, multiple scattering, and the transport equation. The flatland presents a model for the latter process. See [5] for the details. The "flatland" transport equations also presents a model for the wave transport along a surface with random impedance, see, e.g. [6].

Our motivation in this study is to get an insight about the fully three dimensional problem in heterogeneous media with anisotropic scattering: A model which is of interest in radiation oncology, see, e.g. [7–14].

As some basic application domains for the transport type equations one can mention, e.g. nuclear engineering, medical physics (radiation therapy), atmospheric physics and astrophysics. Both in atmospheric and astrophysics, radiative transfer (of photons) is crucial. For a recent monograph on radiative transfer for atmospheric physics see Marshak and Davis (eds) [15]. Radiative transfer also is important in certain aspects of mechanical engineering. Thermal radiative transfer is crucial in the study of flames and furnaces.

In nuclear engineering the study is focusing on certain "isotropy aspects" and homogeneous, "shape-regular", physical domains, and is based on rigorous mathematical development, see, e.g. [16]. On the other hand the radiation therapy application, dealing with biological objects, has started using empirical clinical approaches and advanced to the study of model problems considering media heterogeneity and anisotropic scatterings in complex geometric configurations, viz [7–13,17,14,18]. The mathematical aspects, in this application, are yet to be developed.

A heuristic approach uses asymptotic expansions to transfer the transport integral operator to a diffusion Fokker–Planck operator. A development which requires small angular scattering ($\sigma_s(\theta)$ is peaked about $\theta = 0$). Yet, assuming small angle of flight ($\theta \approx 0$), another asymptotic expansion would yield the Fermi equation, see, e.g. [19–23,1,2,24–26]. Numerical algorithms have been mostly based on Monte Carlo simulations for electron, and partially photon, beams, see, e.g. [27–29,31,30,32,33]. The finite element schemes, based on the idea of the *exact transport + projection* in [34] are considered in [35,4,36,37]. Finally a paraxial approximation for space charged dominated beams is considered in [38].

An outline of this paper is as follows: In Section 2 we give a formal derivation of the "flatland" transport equation from the 3D transport equation. In Section 3, using the 2π periodicity we derive a canonical form of the linear flatland equation and its zeroth (the balance equation), first and second order angular moments. Section 4 is devoted to the beam problem where we give an approximation for the transport cross-section σ_{tr}. In Section 5 we obtain the P_1 approximation, as well as the Fokker–Planck and Fermi developments. In Section 6 we formulate a model problem in bounded medium. In Section 7 we introduce four discretization algorithms. And finally in our concluding Section 8 we give examples of numerical implementations of the discrete problems. Throughout the report, C will denote an absolute constant not necessarily the same at each occurrence, unless otherwise explicitly stated.

2. A formal derivation of the "flatland" transport equation

Let us consider the one-group, 3-D transport equation with isotropic scattering:

$$\sqrt{1-\mu^2}\cos\gamma\frac{\partial\psi}{\partial x}(x,y,z,\mu,\gamma)+\sqrt{1-\mu^2}\sin\gamma\frac{\partial\psi}{\partial y}(x,y,z,\mu,\gamma)$$
$$+\mu\frac{\partial\psi}{\partial z}(x,y,z,\mu,\gamma)+\Sigma_t\psi(x,y,z,\mu,\gamma)$$

$$= \frac{\Sigma_s}{4\pi}\int_0^{2\pi}\int_{-1}^{1}\psi(x,y,z,\mu',\gamma')\,\mathrm{d}\mu'\,\mathrm{d}\gamma' + \frac{1}{4\pi}Q(x,y,z),$$
$$(x,y,z)\in V^3,\ -1\le\mu\le 1,\ -\pi<\gamma\le\pi. \tag{2.1}$$

Here V^3 is a convex 3-D system, μ is the cosine of the angle between the direction of flight and the direction of the positive z-axis, and γ is the (azimuthal) angle between the projection of the direction of flight onto the x, y-plane and the direction of the positive x-axis.

We assume that the system and boundary conditions are such that the solution is independent of z and a symmetric (even) function of μ:

$$\psi(x,y,z,\mu,\gamma)=\psi(x,y,\mu,\gamma)=\psi(x,y,-\mu,\gamma)\equiv\frac{1}{2}\Psi(x,y,\mu,\gamma). \tag{2.2}$$

The factor $1/2$ is included so that

$$\Psi(x,y,\mu,\gamma)=2\psi(x,y,\mu,\gamma)=\psi(x,y,\mu,\gamma)+\psi(x,y,-\mu,\gamma). \tag{2.3}$$

Then Eq. (2.1) simplifies to:

$$\sqrt{1-\mu^2}\cos\gamma\frac{\partial\Psi}{\partial x}(x,y,\mu,\gamma)+\sqrt{1-\mu^2}\sin\gamma\frac{\partial\Psi}{\partial y}(x,y,\mu,\gamma)+\Sigma_t\Psi(x,y,\mu,\gamma)$$
$$=\frac{\Sigma_s}{2\pi}\int_0^{2\pi}\int_0^{1}\Psi(x,y,\mu',\gamma')\,\mathrm{d}\mu'\,\mathrm{d}\gamma'+\frac{1}{2\pi}Q(x,y),$$
$$(x,y)\in V^2,\ 0\le\mu\le 1,\ -\pi<\gamma\le\pi. \tag{2.4}$$

Here V^2 is a convex 2-D system. Eq. (2.4) is equivalent to the standard x, y-geometry transport equation, which has a slightly different definition of the angular variables.

To obtain the "flatland" transport equation, we make the S_2 approximation in μ in Eq. (2.3), but we do not make any approximation in γ. The simplest way to do this is to set $\mu=1/\sqrt{3}$ in Eq. (2.4) and assume:

$$\Psi(x,y,\mu,\gamma)\approx\Psi\left(x,y,\frac{1}{\sqrt{3}},\gamma\right)\equiv\hat{\Psi}(x,y,\gamma)\quad 0\le\mu\le 1. \tag{2.5}$$

Eq. (2.4) becomes:

$$\sqrt{\frac{2}{3}}\left(\cos\gamma\frac{\partial\hat{\Psi}}{\partial x}(x,y,\gamma)+\sin\gamma\frac{\partial\hat{\Psi}}{\partial y}(x,y,\gamma)\right)+\Sigma_t\hat{\Psi}(x,y,\gamma)$$
$$=\frac{\Sigma_s}{2\pi}\int_0^{2\pi}\hat{\Psi}(x,y,\gamma')\,\mathrm{d}\gamma'+\frac{1}{2\pi}Q(x,y),\quad (x,y)\in V^2,\ -\pi<\gamma\le\pi. \tag{2.6}$$

If the factor $\sqrt{2/3}$ were replaced by unity, (2.6) would become the "flatland" transport equation. (The reason for the non-unity value of this factor is that particles travel in the polar directions $\mu=\pm1/\sqrt{3}$ rather than $\mu=0$.) If we rescale the cross sections and source by:

$$\hat{\Sigma}_t\equiv\sqrt{\frac{3}{2}}\Sigma_t,\qquad\hat{\Sigma}_s\equiv\sqrt{\frac{3}{2}}\Sigma_s,\qquad\hat{Q}(x,y)\equiv\sqrt{\frac{3}{2}}Q(x,y), \tag{2.7}$$

then Eq. (2.6) directly reduces to the "flatland" transport equation:

$$\cos\gamma\frac{\partial\hat{\Psi}}{\partial x}(x,y,\gamma)+\sin\gamma\frac{\partial\hat{\Psi}}{\partial y}(x,y,\gamma)+\hat{\Sigma}_t\hat{\Psi}(x,y,\gamma)=\frac{\hat{\Sigma}_s}{2\pi}\int_0^{2\pi}\hat{\Psi}(x,y,\gamma')\,\mathrm{d}\gamma'+\frac{1}{2\pi}\hat{Q}(x,y),$$
$$(x,y)\in V^2,\ -\pi<\gamma\le\pi. \tag{2.8}$$

3. The flatland linear Boltzmann equation

Using some identifications, e.g. $\psi(\cdot,\theta)=\hat{\Psi}(\cdot,\gamma)$, and the 2π periodicity, the *Flatland linear Boltzmann equation* (FLB) (2.8) can be written as:

$$\Omega\cdot\nabla\psi+\bar{\sigma}_a\psi=\int_0^{2\pi}\sigma_s(\theta-\theta')[\psi(\theta')-\psi(\theta)]\,\mathrm{d}\theta'+q(x,y,\theta), \tag{3.1}$$

where $\Omega:=(\cos\theta,\ \sin\theta)$ and $\nabla=(\partial/\partial x,\ \partial/\partial y)$. Introducing the scattering cross section

$$\bar{\sigma}_s:=\int_0^{2\pi}\sigma_s(\theta-\theta')\mathrm{d}\theta, \tag{3.2}$$

and letting $v=\theta-\theta'$, by the 2π periodicity of σ_s, $\int_0^{2\pi}\sigma_s(\theta-\theta')\mathrm{d}\theta=\int_0^{2\pi}\sigma_s(v)\mathrm{d}v$. Thus the Eq. (3.1) can be written as

$$\Omega\cdot\nabla\psi+\bar{\sigma}_a\psi=\int_0^{2\pi}\sigma_s(\theta-\theta')\psi(\theta')\,\mathrm{d}\theta'-\bar{\sigma}_s\psi+q. \tag{3.3}$$

Now we define the total cross section

$$\bar{\sigma}_t:=\bar{\sigma}_a+\bar{\sigma}_s, \tag{3.4}$$

and rewrite the Eq. (3.1) as

$$\Omega\cdot\nabla\psi+\bar{\sigma}_t\psi=\int_0^{2\pi}\sigma_s(\theta-\theta')\psi(\theta')\,\mathrm{d}\theta'+q, \tag{3.5}$$

where $\bar{\sigma}_t\geq\bar{\sigma}_s$ (=only if $\bar{\sigma}_a=0$). Integrating (3.5) over $\theta\in[0,2\pi]$ we get

$$\nabla\cdot J+\bar{\sigma}_t\Psi=\int_0^{2\pi}\bar{\sigma}_s\psi(\theta')\,\mathrm{d}\theta'+Q_0=\bar{\sigma}_s\Psi+Q_0, \tag{3.6}$$

where

$$J=\int_0^{2\pi}\Omega\psi\,\mathrm{d}\theta,\qquad \Psi=\int_0^{2\pi}\psi\,\mathrm{d}\theta,\quad\text{and}\quad Q_0=\int_0^{2\pi}q\,\mathrm{d}\theta. \tag{3.7}$$

Now rearranging the terms in (3.6) we get *the usual balance equation*:

$$\nabla\cdot J+\bar{\sigma}_a\Psi=Q_0. \tag{3.8}$$

We recall that for the *differential scattering* $\sigma_s(\theta)$:

$$\begin{cases}|\theta|<\pi/2: & \text{corresponds to forward scattering}\\ |\theta|=\pi/2: & \text{means ``void'' scattering region}\\ |\theta|>\pi/2: & \text{corresponds to backward scattering.}\end{cases} \tag{3.9}$$

The *symmetry* condition:

$$\sigma_s(\theta)=\sigma_s(-\theta), \tag{3.10}$$

yields an even Fourier series expansion for $\sigma_s(\theta)$ viz,

$$\sigma_s(\theta)=\sum_{n=0}^{\infty}\frac{\sigma_{sn}}{\pi}(\cos n\theta), \tag{3.11}$$

where

$$\sigma_{s0}=\bar{\sigma}_s,\quad\text{and}\quad\sigma_{sm}=\int_0^{2\pi}\sigma_s(\theta)\cos m\theta\,\mathrm{d}\theta. \tag{3.12}$$

Multiply (3.5) by Ω, integrate over θ, and change the order of integrations to get

$$\int_0^{2\pi} \Omega(\Omega\cdot\nabla\psi)\,\mathrm{d}\theta + \bar{\sigma}_t J = \int_{\theta=0}^{2\pi} \Omega\left[\int_{\theta'=0}^{2\pi} \sigma_s(\theta-\theta')\psi(\theta')\,\mathrm{d}\theta'\right]\mathrm{d}\theta + Q_1$$
$$= \int_{\theta'=0}^{2\pi} \psi(\theta')\left[\int_{\theta=0}^{2\pi} \Omega\sigma_s(\theta-\theta')\mathrm{d}\theta\right]\mathrm{d}\theta' + Q_1. \tag{3.13}$$

Further using (3.11) and the orthogonality of the trigonometric functions we have

$$\int_{\theta=0}^{2\pi} \Omega\ \sigma_s(\theta-\theta')\mathrm{d}\theta = \int_{\theta=0}^{2\pi} (\cos\theta,\ \sin\theta)\sum_{n=0}^{\infty}\frac{\sigma_{sn}}{\pi}\cos n(\theta-\theta')\,\mathrm{d}\theta$$
$$= \int_{\theta=0}^{2\pi} (\cos\theta,\ \sin\theta)\sum_{n=0}^{\infty}\frac{\sigma_{sn}}{\pi}[\cos n\theta\cos n\theta' + \sin n\theta\sin n\theta']\,\mathrm{d}\theta$$
$$= \int_{\theta=0}^{2\pi} \left(\cos^2\theta\cos\theta',\ \sin^2\theta\sin\theta'\right)\frac{\sigma_{s1}}{\pi}\,\mathrm{d}\theta$$
$$= \left(\pi\cos\theta',\ \pi\sin\theta'\right)\frac{\sigma_{s1}}{\pi} = \sigma_{s1}(\cos\theta',\ \sin\theta') = \sigma_{s1}\Omega'. \tag{3.14}$$

Inserting (3.14) in (3.13) we thus obtain

$$\int_0^{2\pi} \Omega(\Omega\cdot\nabla\psi)\,\mathrm{d}\theta + \bar{\sigma}_t J = \sigma_{s1}\int_{\theta'=0}^{2\pi}\psi(\theta')\Omega'\,\mathrm{d}\theta' + Q_1 = \sigma_{s1}J + Q_1, \tag{3.15}$$

where

$$Q_1 = \int_0^{2\pi} \Omega q\,\mathrm{d}\theta. \tag{3.16}$$

Now we define *the transport cross-section* viz,

$$\sigma_{\mathrm{tr}} = \bar{\sigma}_t - \sigma_{s1} = \bar{\sigma}_a + \bar{\sigma}_s - \sigma_{s1} = \bar{\sigma}_a + (\sigma_{s0} - \sigma_{s1}). \tag{3.17}$$

Thus we have

$$\int_0^{2\pi} \Omega(\Omega\cdot\nabla\psi)\,\mathrm{d}\theta + \sigma_{\mathrm{tr}} J = Q_1. \tag{3.18}$$

4. A beam problem

Now let us consider a beam problem, with $\bar{\sigma}_a = 0$ (i.e. $\bar{\sigma}_t = \bar{\sigma}_s = \sigma_{s0}$), and:

$$q(x, y, \theta) = \delta(x)\delta(y)\delta(\theta). \tag{4.1}$$

Then the Eq. (3.5) would become

$$\Omega\cdot\nabla\psi + \sigma_{s0}\psi = \int_0^{2\pi}\sigma_s(\theta-\theta')\psi(\theta')\,\mathrm{d}\theta' + \delta(x)\delta(y)\delta(\theta). \tag{4.2}$$

We assume that ψ is compactly supported in $\mathbb{R}^2$: i.e., that

$$\lim_{x\to\pm\infty}\psi(x,\cdot) = \lim_{y\to\pm\infty}\psi(\cdot, y) = 0, \tag{4.3}$$

and transverse integrate (4.2) over $y\in\mathbb{R}$. Now if $\hat{\psi} = \int\psi\,\mathrm{d}y$, then it follows that

$$\cos\theta\frac{\mathrm{d}\hat{\psi}}{\mathrm{d}x} + \sigma_{s0}\hat{\psi} = \int_0^{2\pi}\sigma_s(\theta-\theta')\hat{\psi}(\theta')\,\mathrm{d}\theta' + \delta(x)\delta(\theta). \tag{4.4}$$

Next, we integrate (4.4) over $\theta \in [0_-, 2\pi]$, change the order of integration on the right hand side and use the fact that $\int_0^{2\pi} \sigma_s(\theta - \theta')\,\mathrm{d}\theta = \bar{\sigma}_s = \sigma_{s0}$, to obtain

$$\frac{\mathrm{d}}{\mathrm{d}x}\int_0^{2\pi} (\cos\theta)\hat{\psi}\,\mathrm{d}\theta = \delta(x). \tag{4.5}$$

Thus

$$\int_0^{2\pi} \cos\theta\,\hat{\psi}(x,\theta)\,\mathrm{d}\theta = \begin{cases} 1, & x > 0, \\ 0, & x < 0. \end{cases} \tag{4.6}$$

Now taking the $\cos\theta$ moment of (4.4) yields

$$\begin{aligned} \frac{\mathrm{d}}{\mathrm{d}x}\int_0^{2\pi} \cos^2\theta\,\hat{\psi}\,\mathrm{d}\theta + \sigma_{s0}\int_0^{2\pi} \cos\theta\,\hat{\psi}\,\mathrm{d}\theta &= \int_0^{2\pi}\left[\int_0^{2\pi} \sigma_s(\theta-\theta')\hat{\psi}(\theta')\,\mathrm{d}\theta'\right]\cos\theta\,\mathrm{d}\theta \\ &\quad + \int_0^{2\pi} \cos\theta\delta(\theta)\,\delta(x)\,\mathrm{d}\theta \\ &= \int_0^{2\pi}\left[\int_0^{2\pi} \sigma_s(\theta-\theta')\cos\theta\,\mathrm{d}\theta\right]\hat{\psi}(\theta')\,\mathrm{d}\theta' + \delta(x), \end{aligned} \tag{4.7}$$

where using the 2π-periodicity of σ_s, (3.10) and (3.11) we have that

$$\begin{aligned} \int_0^{2\pi} \sigma_s(\theta-\theta')\cos\theta\,\mathrm{d}\theta &= \int_{-\theta'}^{2\pi-\theta'} \sigma_s(\alpha)\cos(\alpha+\theta')\,\mathrm{d}\alpha \\ &= \int_0^{2\pi} \sigma_s(\alpha)\cos(\alpha)\cos(\theta')\,\mathrm{d}\alpha - \int_0^{2\pi} \sigma_s(\alpha)\sin(\alpha)\sin(\theta')\,\mathrm{d}\alpha \\ &= \cos(\theta')\sigma_{s1}. \end{aligned} \tag{4.8}$$

Hence, inserting (4.8) in (4.7) it follows that

$$\frac{\mathrm{d}}{\mathrm{d}x}\int_0^{2\pi} \cos^2\theta\hat{\psi}\,\mathrm{d}\theta + \sigma_{s0}\int_0^{2\pi} \cos\theta\hat{\psi}\,\mathrm{d}\theta = \sigma_{s1}\int_0^{2\pi} \cos\theta\hat{\psi}\,\mathrm{d}\theta + \delta(x), \tag{4.9}$$

or more concisely,

$$\frac{\mathrm{d}}{\mathrm{d}x}\int_0^{2\pi} \cos^2\theta\hat{\psi}\,\mathrm{d}\theta + \sigma_{\mathrm{tr}}\int_0^{2\pi} \cos\theta\hat{\psi}\,\mathrm{d}\theta = \delta(x). \tag{4.10}$$

Now subtracting the Eq. (4.5) from the (4.10) we get

$$\frac{\mathrm{d}}{\mathrm{d}x}\int_0^{2\pi} (\cos\theta - 1)\cos\theta\,\hat{\psi}\,\mathrm{d}\theta + \sigma_{\mathrm{tr}}\int_0^{2\pi} \cos\theta\hat{\psi}\,\mathrm{d}\theta = 0. \tag{4.11}$$

Thus, for $x > 0$, using (4.6) we have

$$\sigma_{\mathrm{tr}} = \frac{\frac{\mathrm{d}}{\mathrm{d}x}\left(\int_0^{2\pi}(1-\cos\theta)(\cos\theta\,\hat{\psi})\,\mathrm{d}\theta\right)}{\int_0^{2\pi}(\cos\theta\hat{\psi})\,\mathrm{d}\theta} \approx \frac{\frac{\mathrm{d}}{\mathrm{d}x}\left(\int_0^{2\pi}\frac{\theta^2}{2}(\cos\theta\,\hat{\psi})\,\mathrm{d}\theta\right)}{\int_0^{2\pi}(\cos\theta\hat{\psi})\,\mathrm{d}\theta} = \frac{1}{2}\frac{\mathrm{d}}{\mathrm{d}x}\langle\theta^2\rangle.$$

Hence

$$\sigma_{\mathrm{tr}} \approx \frac{1}{2}\frac{\mathrm{d}}{\mathrm{d}x}\langle\theta^2\rangle. \tag{4.12}$$

This is the same result as in the three dimensional case, see [20,1,2].

5. The P_1 approximation

Recalling (3.7) we have the following averaging approximations:

$$\psi(x, y, \theta) \approx \frac{1}{2\pi} [\Psi(x, y) + 2\Omega \cdot J(x, y)]. \tag{5.1}$$

It is easy to check that $\int_0^{2\pi} (\Omega\Omega)\Omega \cdot J(x, y)\, d\theta = 0$. Thus we may write

$$\begin{aligned}\int_0^{2\pi} \Omega\Omega\psi\, d\theta &= \int_0^{2\pi} \Omega\Omega \frac{1}{2\pi} [\Psi(x, y) + 2\Omega \cdot J(x, y)]\, d\theta \\ &\approx \frac{\Psi}{2\pi} \int_0^{2\pi} \Omega\, \Omega\, d\theta = \frac{\Psi}{2\pi} \int_0^{2\pi} (\cos\theta, \sin\theta)(\cos\theta, \sin\theta)\, d\theta \\ &= \frac{\Psi}{2\pi} \int_0^{2\pi} \begin{bmatrix} \cos^2\theta & \cos\theta \sin\theta \\ \cos\theta \sin\theta & \sin^2\theta \end{bmatrix} d\theta = \Psi\left(\frac{1}{2} I\right). \end{aligned} \tag{5.2}$$

Plugging (5.2) in the Eq. (3.18) we get

$$\nabla\Psi\left(\frac{1}{2} I\right) + \sigma_{\text{tr}} J = Q_1, \quad \text{i.e., } \frac{1}{2}\nabla\Psi + \sigma_{\text{tr}} J = Q_1, \tag{5.3}$$

and consequently,

$$J = -\frac{1}{2\sigma_{\text{tr}}}\nabla\Psi + \frac{1}{\sigma_{\text{tr}}} Q_1. \tag{5.4}$$

Inserting (5.4) in the Eq. (3.8) it follows that

$$-\nabla \cdot \left(\frac{1}{2\sigma_{\text{tr}}}\nabla\Psi\right) + \bar{\sigma}_a \Psi = Q_0 - \nabla \cdot \left(\frac{1}{\sigma_{\text{tr}}} Q_1\right). \tag{5.5}$$

Thus in flatland (2-D) the diffusion coefficient is $\frac{1}{2\sigma_{\text{tr}}}$, while in x, y-geometry (3-D transport with 1-D symmetry) the diffusion coefficient is $\frac{1}{3\sigma_{\text{tr}}}$!!

5.1. The Fokker–Planck and Fermi developments

Let us return to Eq. (3.1). Assume that $\sigma_s(\theta)$ is very peaked near $\theta = 0$ (that is: we have very small angular scattering). We let first $q \equiv 0$ and Taylor expand $\psi(\theta')$, on the right hand side of (3.1), about θ, viz,

$$\begin{aligned}\Omega \cdot \nabla\psi + \bar{\sigma}_a\psi &\approx \int_0^{2\pi} \sigma_s(\theta - \theta') \times \left[\psi(x, y, \theta) + (\theta' - \theta)\frac{\partial\psi}{\partial\theta}(x, y, \theta)\right. \\ &\quad \left. + \frac{1}{2}(\theta' - \theta)^2 \frac{\partial^2\psi}{\partial\theta^2}(x, y, \theta) - \psi(x, y, \theta)\right] d\theta' \\ &\approx \left[\frac{1}{2}\int_0^{2\pi} \sigma_s(\theta - \theta')(\theta - \theta')^2\, d\theta'\right] \frac{\partial^2\psi}{\partial\theta^2}, \end{aligned} \tag{5.6}$$

where in the last approximation we use 2π periodicity of σ_s together with the small angular scattering assumption ($\alpha \approx \sin\alpha$) to write,

$$\int_0^{2\pi} \sigma_s(\theta - \theta')(\theta - \theta') d\theta' = \int_0^{2\pi} \sigma_s(\alpha)\alpha\, d\alpha \approx \int_0^{2\pi} \sigma_s(\alpha) \sin\alpha\, d\alpha = 0,$$

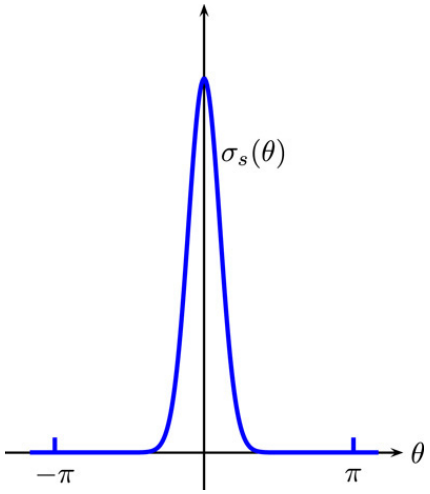

Fig. 1. The Dirac function $\sigma_s(\theta)$.

where in the last step we use the orthogonality and (3.11). A further approximation of the last integral yields, using 2π periodicity, that:

$$\frac{1}{2}\int_0^{2\pi}\sigma_s(\theta-\theta')(\theta-\theta')^2\,\mathrm{d}\theta' = \frac{1}{2}\int_0^{2\pi}\sigma_s(\theta)(\theta)^2\,\mathrm{d}\theta = \int_0^{2\pi}\sigma_s(\theta)\left[1-\left(1-\frac{\theta^2}{2}\right)\right]\mathrm{d}\theta$$
$$\approx \int_0^{2\pi}\sigma_s(\theta)[1-\cos\theta]\,\mathrm{d}\theta = \sigma_{s0}-\sigma_{s1} = \sigma_{\mathrm{tr}}.$$

Hence we have the following development:

$$\Omega\cdot\nabla\psi+\bar{\sigma}_a\psi = \sigma_{\mathrm{tr}}\frac{\partial^2\psi}{\partial\theta^2}+q. \tag{5.7}$$

We point out that the three dimensional correspondence to this development ends up with the angular diffusion coefficient $\sigma_{\mathrm{tr}}/2$, see, e.g. [1,2,25]. The Eq. (5.7) is *the Fokker–Planck approximation*. To this approach we assumed *small angular scattering*, see Fig. 1 below where σ_s is highly peaked about $\theta=0$. To get *The Fermi approximation*, we also assume *small angle of flight* (beam): So in Eq. (5.7) we take $q=0$, $\cos\theta\approx 1$ and $\sin\theta\approx\theta$, (see, e.g. [10]), to get

$$\frac{\partial\psi}{\partial x}+\theta\frac{\partial\psi}{\partial y}+\bar{\sigma}_a\psi = \sigma_{\mathrm{tr}}\frac{\partial^2\psi}{\partial\theta^2}, \quad -\pi<\theta<\pi. \tag{5.8}$$

Once again we point out that the three dimensional version of the Fermi equation has the diffusion coefficient $\sigma_{\mathrm{tr}}/2$, rather than σ_{tr} in here. Now let us see if we can adopt Pomraning's [24] derivation of the three dimensional Fokker–Planck operator:

$$\mathcal{L}\psi(\theta) = \int_0^{2\pi}\sigma_s(\theta-\theta')\,\psi(\theta')\,\mathrm{d}\theta' - \sigma_{s0}\psi(\theta). \tag{5.9}$$

Recalling (3.12) we use the following approximation procedure:

$$\sigma_{sn} = \int_0^{2\pi}\sigma_s(\theta)\cos n\theta\,\mathrm{d}\theta \approx \int_{-\pi}^{\pi}\sigma_s(\theta)\left[1-\frac{n^2\theta^2}{2}\right]\mathrm{d}\theta$$
$$= \int_{-\pi}^{\pi}\sigma_s(\theta)\left\{1-n^2\left[1-\left(1-\frac{\theta^2}{2}\right)\right]\right\}\mathrm{d}\theta$$
$$\approx \int_{-\pi}^{\pi}\sigma_s(\theta)\left\{1-n^2\left[1-\cos\theta\right]\right\}\mathrm{d}\theta = \sigma_{s0}-n^2(\sigma_{s0}-\sigma_{s1}). \tag{5.10}$$

Thus the differential cross section, see (3.11), is approximated viz,

$$\sigma_s(\theta) = \sum_{n=0}^{\infty} \frac{\sigma_{sn}}{\pi} (\cos n\theta) \approx \sum_{n=0}^{\infty} \frac{1}{\pi} \left[\sigma_{s0} - n^2(\sigma_{s0} - \sigma_{s1})\right] \cos n\theta, \tag{5.11}$$

and hence we have

$$\begin{aligned}
\int_0^{2\pi} \sigma_s(\theta - \theta')\, \psi(\theta')\, \mathrm{d}\theta' &\approx \sum_{n=0}^{\infty} \frac{1}{\pi} \int_0^{2\pi} [\sigma_{s0} - n^2(\sigma_{s0} - \sigma_{s1})] \cos n(\theta - \theta')\psi(\theta')\, \mathrm{d}\theta' \\
&= \sigma_{s0} \left[\frac{1}{\pi} \sum_{n=0}^{\infty} \int_0^{2\pi} \cos n(\theta - \theta')\psi(\theta')\, \mathrm{d}\theta'\right] \\
&\quad + \sigma_{\mathrm{tr}} \left[-\frac{1}{\pi} \sum_{n=0}^{\infty} n^2 \int_0^{2\pi} \cos n(\theta - \theta')\psi(\theta')\, \mathrm{d}\theta'\right] \\
&= \left(\sigma_{s0} + \sigma_{\mathrm{tr}} \frac{\partial^2}{\partial\theta^2}\right) \Phi(\theta),
\end{aligned}$$

where, changing the order of integration in $\cos k(\theta - \theta')$ moment, we have

$$\Phi(\theta) := \frac{1}{\pi} \sum_{n=0}^{\infty} \int_0^{2\pi} \cos n(\theta - \theta')\psi(\theta')\mathrm{d}\theta' \equiv \psi(\theta). \tag{5.12}$$

Now recalling (5.9) it follows that

$$\mathcal{L}\psi(\theta) \approx \sigma_{s0}\psi(\theta) + \sigma_{\mathrm{tr}} \frac{\partial^2}{\partial\theta^2}\psi(\theta) - \sigma_{s0}\psi(\theta) = \sigma_{\mathrm{tr}} \frac{\partial^2}{\partial\theta^2}\psi(\theta). \tag{5.13}$$

Once again we have confirmed the angular diffusion coefficient σ_{tr} for the flatland case, versus the $\sigma_{\mathrm{tr}}/2$ of the 3-D case. Pomraning's approach in [24] can be viewed as an angular peaking of a Gaussian $\mathrm{e}^{-\theta^2}$ from an algebraic fall off to an exponential one as in Figs. 1 and 2.

6. A model problem for the current

The Eqs. (5.7) and (5.8) are formulated for the flux ψ, a measure of interest to nuclear engineers. In medical physics the quantity of interest: dose (energy deposited per unit mass, see [17,8–13]) is related to the current function

$$\phi = (\cos\theta)\psi. \tag{6.1}$$

Assuming forward peakedness ($-\pi/2 \le \theta \le \pi/2$), and using the scaling substitution

$$z = \tan(\theta), \quad \theta \in (-\pi/2, \pi/2), \tag{6.2}$$

we introduce the scaled current function φ as

$$\varphi(x, y, z) \equiv \frac{\phi(x, y, \tan^{-1} z)}{(1 + z^2)}. \tag{6.3}$$

Note that now z corresponds to the angular variable θ. Below, we shall keep θ away from the poles $\pm\pi/2$, and correspondingly formulate a problem for the current function φ, in the bounded domain $Q \equiv I_x \times I_y \times I_z := [0, L] \times [-y_0, y_0] \times [-z_0, z_0]$:

$$\begin{cases}
\varphi_x + z\varphi_y = \varepsilon A\, \varphi, & (x, x_\perp) \in Q, \\
\varphi_z(x, y, \pm z_0) = 0, & (x, y) \in I_x \times I_y, \\
\varphi(x, \pm y_0, z) = 0, & \text{on } \tilde{\Gamma}^-_{\tilde{\beta}} \setminus \{\text{supp } f\}, \\
\varphi(0, x_\perp) = f(x_\perp), &
\end{cases} \tag{6.4}$$

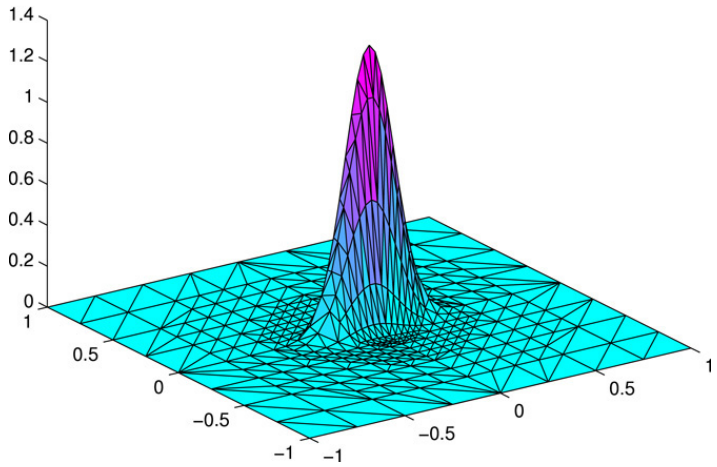

Fig. 2. The closed form exact solution at $x = 20$.

where $\tilde{\Gamma}^-_{\tilde{\beta}} := \{(x, x_\perp) \in \partial Q : \tilde{\beta} \cdot \boldsymbol{n} < 0\}$, $\tilde{\beta} = (1, z, 0)$, and $x_\perp \equiv (y, z)$ is the transversal variable, $\boldsymbol{n} := n(x, x_\perp)$ is the outward unit normal to $\tilde{\Gamma}$ at $(x, x_\perp) \in \tilde{\Gamma}$. Further we use $\varepsilon := \sigma_{\text{tr}}(x, y)$, and we have replaced the product of δ-functions at the boundary by a L_2-function f (source term). The diffusion operator in (6.4) is

$$\begin{cases} A = \partial^2/\partial z^2, & \text{Fermi,} \\ A\cdot = \partial/\partial z[a(z)\partial/\partial z(b(z)\cdot)], & \text{Fokker–Planck,} \end{cases} \tag{6.5}$$

where $a(z) = 1 + z^2$ and $b(z) = (1 + z^2)^{3/2}$. In the following section we give four Galerkin type numerical algorithms for the Fermi case. Detailed numerical analysis for these schemes, for both equations, can be found in [35,4,36,37].

The Fermi equation is modeling the penetration (in the direction of the x-axis) of a narrowly focused pencil beam, incident at the transversal boundary of an *isotropic* slab, entering to the domain at the point $(x, y, z) = (0, 0, 0)$. The three dimensional Fermi equation is one of the basic equations of medical physics behind radiation therapy.

Mathematically, our model problem corresponds to a forward–backward (z changes the sign), convection dominated (ε is small), convection–diffusion equation of the degenerate type (convection in x, y and diffusion in z).

7. The discretization algorithms

The semidiscrete schemes. In this part we consider two semidiscrete schemes where the problem Eq. (6.4) is discretized in the variable $x_\perp := (y, z)$ by the *Standard Galerkin* (SG) and the *Semi-Streamline Diffusion* (SSD), finite element methods.

Because of the structure of the equation, the penetrating variable x is interpreted as a time variable and treated by usual time discretization schemes, such as *backward Euler* and *Crank–Nicholson*, leading to the fully discrete schemes.

We emphasis that the SSD method is performed only on the $x_\perp$ variable, whereas the usual streamline diffusion (SD) finite element method is applied for the whole $(x, x_\perp)$ domain, see, e.g. [37].

7.1. Standard Galerkin

We discretize in $x_\perp = (y, z)$ using a finite element approximation based on a quasi-uniform triangulation of the domain $I_\perp = I_y \times I_z$ with a mesh size h. We also consider adaptive meshes with refinements in the center. We let $\beta = (z, 0)$ and define the inflow (outflow) boundary as

$$\Gamma^{-(+)}_\beta := \{x_\perp \in \Gamma := \partial I_\perp : \boldsymbol{n}(x_\perp) \cdot \beta < 0\ (>0)\}, \tag{7.1}$$

where $\boldsymbol{n}(x_\perp)$ is the outward unit normal to the boundary Γ at $x_\perp \in \Gamma$. Now, we introduce a discrete, finite dimensional, function space $V_{h,\beta} \subset H^r_\beta(I_\perp)$ with,

$$H^r_\beta(I_\perp) = \{v \in H^r(I_\perp) : v_z(\pm z_0) = 0 \text{ and } v = 0 \text{ on } \Gamma^-_\beta\}, \tag{7.2}$$

where $H^r(I_\perp)$ is the space of all $L_2(I_\perp)$ integrable functions having their first r partial derivatives in $L_2(I_\perp)$. An example of such $V_{h,\beta}$ is the set of sufficiently smooth piecewise polynomials $P(x_\perp)$ of degree $\leq r$, satisfying the boundary conditions in Eq. (6.4). We then seek $\varphi_h \in V_{h,\beta}$, such that

$$\begin{cases} (\varphi_{h,x}, \chi)_\perp + (z\varphi_{h,y}, \chi)_\perp + (\varepsilon\varphi_{h,z}, \chi_z)_\perp = 0, & \forall \chi \in V_{h,\beta}, \\ \varphi_h(0, x_\perp) = f_h(x_\perp), \end{cases} \tag{7.3}$$

where f_h is a finite element approximation of f and the mesh size h is chosen as:

$$h^2 \leq \varepsilon \leq h. \tag{7.4}$$

Here,

$$(u, v)_\perp = \int_{I_\perp} u(x_\perp)v(x_\perp)\,\mathrm{d}x_\perp, \quad \text{and} \quad \|u\|_{L_2(I_\perp)} = (u, u)^{1/2}_\perp.$$

With these assumptions and φ and φ_h being the solutions of (6.4) and (7.3), respectively, we can drive the (continuous and discrete) *stability* estimate, viz

$$\max\left(\sup_{x\in I_x} \|\varphi(x, \cdot)\|_{L_2(I_\perp)}, \sup_{x\in I_x} \|\varphi_h(x, \cdot)\|_{L_2(I_\perp)}\right) \leq \|f\|_{L_2(I_\perp)}. \tag{7.5}$$

For $\varphi \in H^r(\Omega)$ and $\varepsilon \sim h$ the corresponding *convergence rate* is given by,

$$\|\varphi - \varphi_h\|_{L_2(\Omega)} \leq Ch^{r-1}\|\varphi\|_r, \tag{7.6}$$

where $C = C(\Omega, f)$, and $\|\cdot\|_s$, with s being a positive integer, denotes the *Sobolev* norm of functions that are square integrable along with all their partial derivatives of order $\leq s$. For the details and proofs, see, [35].

7.2. A semi streamline diffusion method

Basically, the Streamline Diffusion method is designed for generating *artificial-diffusion* (smoothing) for problems with small or no diffusion. Below, we construct a semi Streamline Diffusion (SSD) scheme with diffusion generating test functions in the y and z directions. This scheme is strongly stable, its smoothing behavior can be seen in the implementation section. The convergence rates are at least as good as in the SG scheme, see, e.g. [37].

Using the SSD we obtain a non-degenerate type convection dominated convection–diffusion, equation with somewhat improved regularity. The test functions having the form $v + \delta v_\beta$ automatically add up the extra diffusion term $\delta(v_\beta, v_\beta)$ to the variational formulation, which combined with $(v, -\varepsilon v_{zz}) = (\varepsilon v_z, v_z)$ leads to a non-degenerate fully diffusive equation (x is interpreted as a time variable). If $\delta \geq \varepsilon$ the diffusion term is of order ε. We assume that $\delta \sim h \geq \varepsilon$, $\beta = (z, 0)$, $v_\beta = \beta \cdot \nabla_\perp v$ and $\nabla_\perp = (\partial/\partial y, \partial/\partial z)$, and v satisfies the boundary conditions in Eq. (6.4). Multiplying the equation in (6.4) by $v + \delta v_\beta$ and integrating over $I_\perp$ we get the SSD scheme,

$$\begin{aligned}(\varphi_x + \varphi_\beta - \epsilon\varphi_{zz}, v + \delta v_\beta)_\perp &= (\varphi_x, v)_\perp + \delta(\varphi_x, v_\beta)_\perp + (\varphi_\beta, v)_\perp \\ &\quad + \delta(\varphi_\beta, v_\beta)_\perp + (\epsilon\varphi_z, v_z)_\perp + \delta(\epsilon\varphi_z, (v_\beta)_z)_\perp = 0.\end{aligned} \tag{7.7}$$

With a symmetry assumption on the transversal plane viz,

$$\|\varepsilon^{1/2}\varphi_z\|_{I_\perp} \sim \|\varepsilon^{1/2}\varphi_y\|_{I_\perp}, \tag{7.8}$$

the scheme (7.7) satisfies the following stability estimate:

Lemma 7.1. *Assuming (7.8) and with $\delta > \varepsilon$ we have that*

$$\|\varphi(L,\cdot)\|^2_{L_2(I_\perp)} + \delta\|\varepsilon^{1/2}\varphi_z(L,\cdot)\|^2_{L_2(I_\perp)} \le \|f\|^2_{L_2(I_\perp)} + \delta\|\varepsilon^{1/2} f_z\|^2_{L_2(I_\perp)}. \tag{7.9}$$

The fully discrete problem. In this section we derive an algorithm which combines the SSD scheme for $I_\perp$ with the backward Euler (BE) method for I_x. In this way, we consider the penetration variable x as a time variable in similar time dependent problems. We split the SSD variational formulation (7.7) as follows:

$$a(\varphi, v) := (\varphi_\beta, v)_{I_\perp} + \delta(\varphi_\beta, v_\beta)_{I_\perp} + (\varepsilon\varphi_z, v_z)_{I_\perp} + \delta(\varepsilon\varphi_z, (v_\beta)_z)_{I_\perp}, \tag{7.10}$$

$$b(\varphi, v) := \delta(\varphi, v_\beta)_{I_\perp} + (\varphi, v)_{I_\perp}, \tag{7.11}$$

and rewrite the problem as: find a solution $\varphi \in H^1_\beta(I_\perp)$ such that

$$b(\varphi_x, v) + a(\varphi, v) = 0, \quad \forall v \in H^1_\beta(I_\perp). \tag{7.12}$$

We use the finite dimensional subspace, $V_{h,\beta}$ of $H^1_\beta(I_\perp)$ and replace the discrete solution φ_h with the "space–time-discrete" ansatz

$$\varphi_h(x, y, z) = \sum_{j=1}^{M} \xi_j(x)\zeta_j(y, z), \tag{7.13}$$

where $M \sim 1/h$. We insert (7.13) into the semidiscrete counterpart of (7.12) and replace v by ζ_i for $i = 1, \ldots, M$. This gives the discretization scheme

$$\sum_{j=1}^{M} \xi_j'(x) b(\zeta_i, \zeta_j) + \sum_{j=1}^{M} \xi_j(x) a(\zeta_i, \zeta_j) = 0, \quad i = 1, \ldots, M,$$

with the matrix form,

$$B\Xi'(x) + A\Xi(x) = 0 \tag{7.14}$$

where $B = (b_{ij})$ with entries $b_{ij} = b(\zeta_i, \zeta_j)$, $A = (a_{ij})$ with entries $a_{ij} = a(\zeta_i, \zeta_j)$ and $\Xi = (\xi_j)$. Now we use backward Euler to discretize in x and get the fully discrete scheme:

$$B(\Phi_h^n - \Phi_h^{n-1}) + k_n A \Phi_h^n = 0. \tag{7.15}$$

Other fully discrete schemes can be obtained depending on the choice of the discretization method in x, e.g. Crank Nicholson, or discontinuous Galerkin.

Characteristic schemes for non-degenerate problem. The main feature in this part is the idea of *exact transport+ projection*, see [34]. To illustrate this idea, we consider a homogeneous infinite slab, $\tilde{Q} = (x, y, z)$ of thickness L, $(0 < x < L,\ y, z \in \mathbb{R})$. Let $\{x_n\}$ be an increasing sequence of discrete points and for each n, $\{\mathcal{V}_n\}$ a sequence of piecewise polynomial space on mesh $\{\mathcal{T}_n\}$ on the transversal domain $I_\perp$. Given the approximate solution $\varphi^{h,n} \in \mathcal{V}_n$ at the collision site x_n, solve the pencil beam equation exactly on the interval (x_n, x_{n+1}) with the data $\varphi^{h,n}$ to give the solution $\varphi_-^{h,n+1}$ at x_{n+1}. This is an exact transport procedure. Now, one may compute $\varphi^{h,n+1} = \mathcal{P}_{n+1}\varphi_-^{h,n+1}$, with $\mathcal{P}_{n+1}$ being a projection into $\mathcal{V}_{n+1}$. One may interpret $\varphi^{h,n+1}$ as the post collision solution at (the other face of collision) x_{n+1}. In this way, we have an algorithm of type *exact transport+projection*. More precisely:

The domain $Q := I_x \times I_y \times I_z$ is subdivided into slabs $S_n := I_x^n \times I_y \times I_z$, with $I_x^n := (x_{n-1}, x_n]$, $n = 1, 2 \ldots, N$. Each slab S_n has its own incident-transversal finite element mesh $\hat{\mathcal{T}}_n$. Consequently, at each x_n we have two transversal meshes $\hat{\mathcal{T}_n^-} = \hat{\mathcal{T}}_n|_{x_n}$ and $\hat{\mathcal{T}_n^+} = \hat{\mathcal{T}_{n+1}}|_{x_n}$. In general $\hat{\mathcal{T}_n^-} \neq \hat{\mathcal{T}_n^+}$ and the passage of information from one slab to the next is performed through a modified L_2-projection. Again, as in the previous section, x is treated like a time variable.

To proceed, we recall that our model problem (6.4) is a, forward–backward, convection dominated convection–diffusion equation of degenerate type. A corresponding non-degenerate equation reads

$$\mathcal{L}(\varphi) := \varphi_x + \beta \cdot \nabla_\perp \varphi - \varepsilon \Delta_\perp \varphi = 0, \tag{7.16}$$

where $\Delta_\perp := \partial^2/\partial y^2 + \partial^2/\partial z^2$ is the transversal Laplacian and $\beta \equiv (z, 0)$.

We introduce the change of coordinates $(x, \bar{x}_\perp) = (x, x_\perp - x\beta)$ and set $\bar{\varphi}(x, \bar{x}_\perp) = \varphi(x, x_\perp)$. The we may reformulate (7.16) as

$$\bar{\varphi}_x - \varepsilon \Delta_\perp \bar{\varphi} = 0, \quad \text{in } [0, L] \times I_y \times I_z, \qquad \bar{\varphi}(0, \bar{x}_\perp) = f(x_\perp). \tag{7.17}$$

Since $\frac{\partial \bar{\varphi}}{\partial x} = \frac{\partial}{\partial x}\varphi(x, \bar{x}_\perp + x\beta) = \frac{\partial \varphi}{\partial x} + \beta \cdot \nabla_\perp \varphi$, for $\varepsilon = 0$, the solution of (7.17) is

$$\bar{\varphi}(x, \bar{x}_\perp) = f(x_\perp - x\beta). \tag{7.18}$$

The characteristics of Eq. (7.17), in the case of $\varepsilon = 0$ are given by $\bar{x}_\perp + x\beta > 0$, and in this case the solution $\varphi(x, \bar{x}_\perp)$ is constant along the characteristics.

7.3. Characteristic Galerkin

In this part we let $\{x_n\}$, $n = 0, 1, \ldots, N$, be an increasing sequence of x values with $x_0 = 0$, and for each $0 \le n \le N$, let $\{\mathcal{T}_n\}$ be the corresponding sequence of triangulations $\mathcal{T}_n$ of $\{x_n\} \times I_y \times I_z$ into triangles K. Furthermore we let $\mathcal{V}_n$ be the space of continuous piecewise linear functions on $\mathcal{T}_n$, i.e. $\mathcal{V}_n = \{v \in \mathcal{C}(I_y \times I_z) : v \text{linear on } K, K \in \mathcal{T}_n\}$, where $\mathcal{C}(D)$ denotes the set of continuous functions on domain D.

Now we consider a pure convection case ($\varepsilon = 0$). Then the characteristic Galerkin (CG) is formulated as follows: For $n = 1, 2 \ldots, N$: find $\varphi^{h,n} \in \mathcal{V}_n$ such that:

$$\int_{I_y \times I_z} \varphi^{h,n}(x_\perp) v(x_\perp)\, \mathrm{d}x_\perp = \int_{I_y \times I_z} \varphi^{h,n-1}(x_\perp - \hbar_n \beta) v(x_\perp)\, \mathrm{d}x_\perp, \tag{7.19}$$

where $\hbar_n = x_n - x_{n-1}$ and $u^{h,0} = f$. In other words

$$\varphi^{h,n} = \mathcal{P}_n T_n \varphi^{h,n-1}, \tag{7.20}$$

where $\mathcal{P}_n : L_2(I_y \times I_z) \to \mathcal{V}_n$ is the L_2 projection defined by $(\mathcal{P}_n w, v) = (w, v)$, $v \in \mathcal{V}_n$, $(\cdot, \cdot)$ is the inner product in $L_2(I_y \times I_z)$, and $T_n \eta(x_\perp) = \eta(x_\perp - \hbar_n \beta)$.

7.4. Characteristic streamline diffusion

The Characteristic Streamline Diffusion (CSD) method is a special case of the Streamline Diffusion (SD) method obtained with oriented phase-space mesh elements. We start constructing a SD mesh: For $n = 1, \ldots, N$, let $\tilde{\mathcal{T}}_n = \{\tilde{K}\}$ be a finite element subdivision of the slab $S_n = I_x^n \times I_y \times I_z$, $I_x^n = (x_{n-1}, x_n)$, into elements $\tilde{K}$. Let $\tilde{\mathcal{V}}_n$ be a space of piecewise polynomials (continuous in $x_\perp$, and with possible discontinuities at the collision sites x_n) on $\tilde{\mathcal{T}}_n$ of degree at most k. For $k = 1$ and small ε, the SD-method may be formulated as follows: For $n = 1, \ldots, N$, find $\tilde{\varphi}^h \equiv \tilde{\varphi}^h | S_n \in \hat{\mathcal{V}}_n$ such that

$$\int_{S_n} (\tilde{\beta} \cdot \nabla \tilde{\varphi}^h)(v + \delta(v_x + \beta \cdot \nabla_\perp v))\, \mathrm{d}x \mathrm{d}x_\perp + \int_{S_n} \varepsilon \nabla_\perp \tilde{\varphi}^h \cdot \nabla_\perp v\, \mathrm{d}x \mathrm{d}x_\perp + \int_{I_\perp} \tilde{\varphi}_+^{h,n} v_+^n\, \mathrm{d}x_\perp$$
$$= \int_{I_\perp} \tilde{\varphi}_-^{h,n} v_+^n\, \mathrm{d}x_\perp, \quad \forall v \in \tilde{\mathcal{V}}_n,$$

where $v_\pm^n(x_\perp) = \lim_{\Delta x \to 0} v(x_n \pm \Delta x, x_\perp)$, $\delta(v_x + \beta \cdot \nabla_\perp v)$ is the streamline diffusion modification, and $\delta \sim h$. In the presence of shock the ε term has a rather involved shock-capturing modification, see [4]

The CSD is obtained making a special choice of the finite element subdivision $\hat{\mathcal{T}}_n = \{\hat{K}\}$ of S_n given by the prismatic elements oriented along the characteristics

$$\hat{K}_n = \{(x, \bar{x}_\perp + (x - x_n)\beta) : \bar{x}_\perp \in K \in \mathcal{T}_n, x \in I_x^n\},$$

where $\mathcal{T}_n = \{K\}$ is a triangulation of $I_\perp$ given above, and now $\hat{\mathcal{V}}_n$ is defined by

$$\hat{\mathcal{V}}_n = \{\hat{v} \in \mathcal{C}(S_n) : \hat{v}(x, x_\perp) = v(x_\perp - (x - x_n)\beta), v \in \mathcal{V}_n\},$$

with $\mathcal{V}_n$ the space of continuous piecewise linear functions on $\mathcal{T}_n$. So $\hat{\mathcal{V}}_n$ consists of the continuous functions $\hat{v}(x, x_\perp)$ on S_n such that $\hat{v}$ is constant along characteristics $x_\perp = \bar{x}_\perp + x\beta$ parallel to the sides of the prismatic elements $\hat{K}_n$. With this choice, we notice that if $\hat{v} \in \hat{\mathcal{V}}_n$, then $\hat{v}_x + \beta \cdot \nabla_\perp \hat{v} = 0$, $(\tilde{\beta} \cdot \nabla \tilde{\varphi}^h = 0)$. The SD-method is then reduced to the following: For $n = 1, \ldots, N$, find $\hat{\varphi}^h \in \hat{\mathcal{V}}_n$ such that

$$\int_{S_n} \hat{\varepsilon} \nabla_\perp \hat{\varphi}^h \cdot \nabla_\perp v \, \mathrm{d}x \mathrm{d}x_\perp + \int_{I_\perp} \hat{\varphi}_+^{h,n} v_+^n \, \mathrm{d}x_\perp = \int_{I_\perp} \hat{\varphi}_-^{h,n} v_+^n \, \mathrm{d}x_\perp, \quad \forall \hat{v} \in \hat{\mathcal{V}}_n, \tag{7.21}$$

where in simple cases $\hat{\varepsilon} = \varepsilon$ and in the presence of shock it involves a shock-capturing modification as $\hat{\varepsilon} = \max(\varepsilon, \mathcal{F}(h^\alpha(|[\hat{\varphi}^h]|/\hbar_n))/M_n)$, with $\mathcal{F}(w)$ being the element-wise average of w, $[v^n] = v_+^n - v_-^n$, $0 < \alpha < 2$, and $M_n = \max_{x_\perp} |\varphi_+^{h,n}(x_\perp)|$. Further $h(x, x_\perp) = h_n(x_\perp - (x - x_n)\beta)$; $h_n(x_\perp)$ gives the local element size of $\mathcal{T}_n$, see, e.g. [34] for details. If ε is small, then (7.21) can be stated as:

$$\int_{I_\perp} \hat{\varepsilon} \nabla_\perp \hat{\varphi}_+^{h,n} \cdot \nabla_\perp v \, \mathrm{d}x_\perp + \int_{I_\perp} \hat{\varphi}_+^{h,n} v \, \mathrm{d}x_\perp = \int_{I_\perp} \hat{\varphi}_-^{h,n} v \, \mathrm{d}x_\perp, \quad \forall \hat{v} \in \mathcal{V}_n. \tag{7.22}$$

Writing $\hat{\varphi}_+^{h,n} = \varphi^{h,n}$, since $\hat{\varphi}_-^{h,n} = T_n \varphi^{h,n-1}$, then $\hat{\varepsilon} = \mathcal{F}(h_n^\alpha |\varphi^{h,n} - T_n \varphi^{h,n-1}|)/M_n$, and we can restate (7.22) as follows: For $n = 1, \ldots, N$, find $\varphi^{h,n} \in \mathcal{V}_n$ such that

$$\int_{I_\perp} \hat{\varepsilon} \nabla_\perp \varphi^{h,n} \cdot \nabla_\perp v \, \mathrm{d}x_\perp + \int_{I_\perp} \varphi^{h,n} v \, \mathrm{d}x_\perp = \int_{I_\perp} T_n \varphi^{h,n-1} v \, \mathrm{d}x_\perp, \quad \forall \hat{v} \in \mathcal{V}_n, \tag{7.23}$$

where $\varphi^{h,0} = f$. We introduce the operator $\hat{\mathcal{P}}_n : L_2(I_\perp) \bigcap L_\infty(I_\perp) \to \mathcal{V}_n$ defined by

$$(\hat{\mathcal{P}}_n w, v) + (\hat{\varepsilon} \nabla_\perp \hat{\mathcal{P}}_n w, \nabla_\perp v) = (w, v), \quad \forall v \in \hat{\mathcal{P}}_n, \tag{7.24}$$

where $\hat{\varepsilon} = \mathcal{F}(h_n^\alpha |\hat{\mathcal{P}}_n w - w|/\max |\hat{\mathcal{P}}_n w|)$, and $(\cdot, \cdot)$ denoting the $L_2(I_\perp)^m$ inner product with $m = 1, 2$. Now we can reformulate (7.22) as

$$\varphi^{h,n} = \hat{\mathcal{P}}_n T_n \varphi^{h,n-1}. \tag{7.25}$$

Hence $\hat{\mathcal{P}}_n$ may be viewed as a modification of the usual L_2 projection, obtained by adding the artificial viscosity term with coefficient $\hat{\varepsilon}$ as defined above.

8. Implementations

We have used the following implementations: To justify the results for SG and SSD, we first discretize the domain $I_\perp = I_y \times I_z$ using the $cG(1)$ method: continuous Galerkin approximation with piecewise linears, and then step advance in x using the Backward Euler (BE) method. As for the characteristics schemes CG and CSD, we allow jump discontinuities in x: we discretize $I_\perp$ using $cG(1)$ and we step advance in x using discontinuous Galerkin approximation with piecewise constants: $dG(0)$.

Let $\varepsilon = \varepsilon(x)$, then the problem (6.4) has the closed form exact solution, see [10],

$$\varphi(x, y, z) = \frac{\sqrt{3}}{\pi \varepsilon x^2} \mathrm{e}^{-2(3(y/x)^2 - 3(y/2)z + z^2)/(\varepsilon x)}. \tag{8.1}$$

This allows us to compare the computed solution with the exact one and derive errors in various norms. However, the throughout comparisons are limited because of the following two reasons: (i) the closed form exact solution (8.1) displays singularities near the origin. (ii) the initial condition used to derive (8.1), being a Dirac δ function, is not numerically realizable. For comparison purposes, we have considered three types of, numerically providable, initial conditions that approximate the Dirac δ function in the L_1 sense: *Maxwellian*, *Hyperbolic*, and *modified Dirac*.

8.1. Mesh

The meshes used in the numerical experiments are shown in Fig. 3. The finest mesh used has a step size of $h = 0.0625$ in the y and z variables, and $k = 0.005$ in the x variable, corresponding to 8198 nodes in two dimensions.

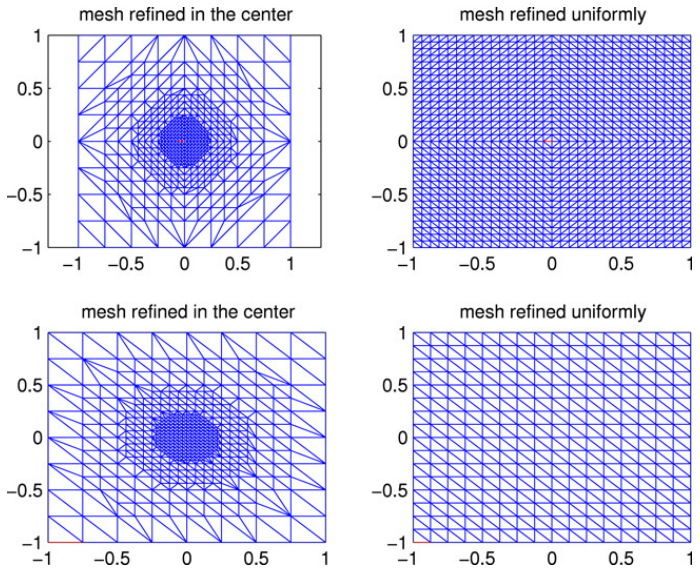

Fig. 3. Meshes used: symmetric refinements (the 2 top figures). Non-symmetric refinements (the remaining 2 "down" figures).

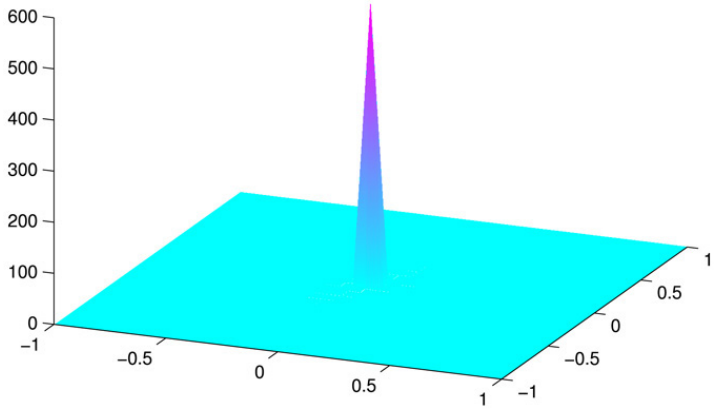

Fig. 4. Closed form exact solution at $x = 1$.

8.2. *Computed solutions*

The computational parameters used rely on the theoretical assumptions in the previous sections: $h^2 < \varepsilon < h$, and $\delta \sim h$. For the computed solutions in the figures we use the values $\varepsilon = 0.002$, and $h = 0.175$ ($h = 0.0625$ in the finest mesh). In SSD and CSD we have chosen $\delta = h/2$. The norms are calculated at $x = 1$ and over $I_\perp$(for the exact solution at $x = 1$ see Fig. 4).

The computed solutions in Figs. 5 and 6 are for CSD and SSD, respectively, where we used the modified Dirac initial data. In the characteristic schemes, x is interpreted as time, with a step chosen as $k = 0.01$. While in the fully discrete schemes, it was set to $k = 0.005$.

The SG method produces layers and the CG has oscillatory behavior, whereas, in most cases, SSD and CSD seem to be more stable. Layers and oscillatory behaviors are eliminated using modified L_2 projections derived in Section 6: Figs. 7 and 8 show the formation of layer for Maxwellian initial data and the oscillatory behavior in the case of a hyperbolic initial condition, respectively. Fig. 9 shows the improved (boundary layer is removed) solution with the Maxwellian initial data, obtained after performing 3 step of modified L_2 projections. The formation of layers can also be avoided using small steps in the penetration direction. Even the oscillating behavior can be removed using the modified L_2 projections. For further implementation results of these types, see [40]. The whole numerical computations are performed using DOLFIN code implemented in C++, viz [39].

Tables 1–3, show the L_∞, L_1, and L_2 norms of the errors between the "exact" and computed solutions for the three initial conditions at $x = 1$. L_2 is the most natural norm for the finite element approaches, because variational

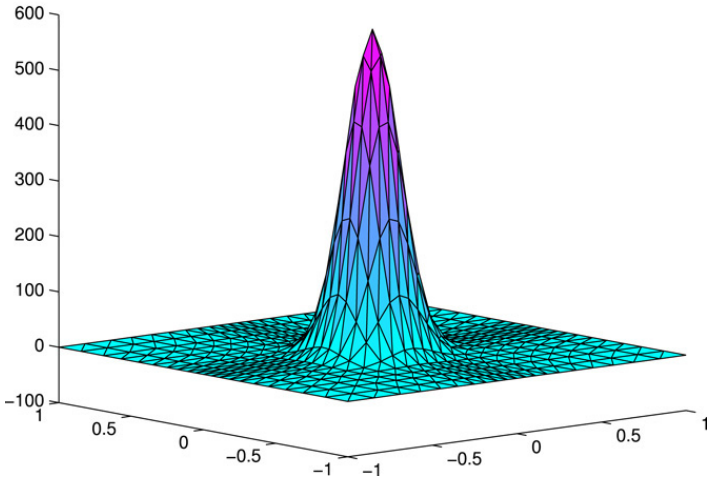

Fig. 5. Computed solution at $x = 1$ with Dirac Init.cond. using CSD.

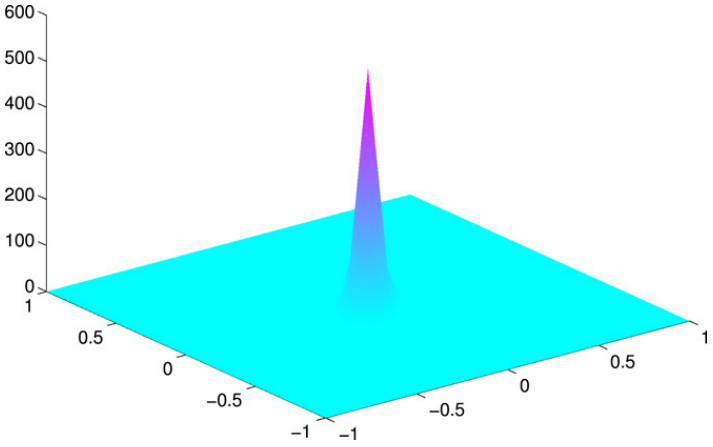

Fig. 6. Computed solution at $x = 1$ with Dirac Init.cond. using SSD.

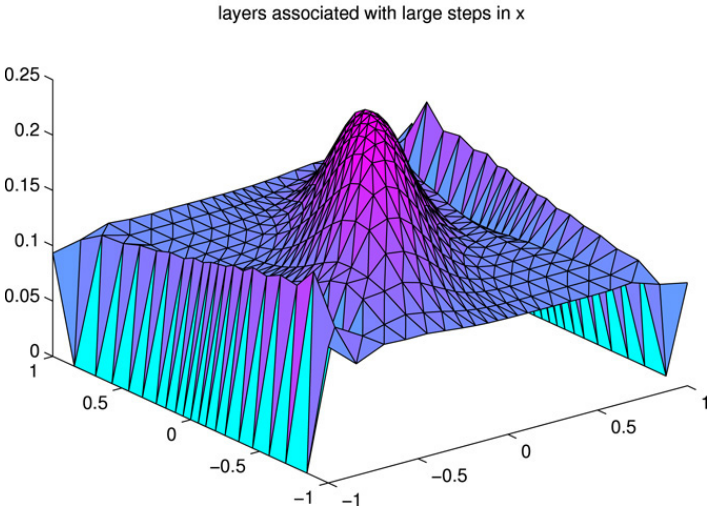

Fig. 7. Formation of layers in a solution with Maxwellian i.c. at $x = 0.66$.

formulation can be interpreted as a scalar product. Therefore even in this limited study we observe the superiority of the L_2 estimates as well as the slight improvements in the L_2 norm due to use of SSD and CSD (see Table 3). $\tilde{L}_2$

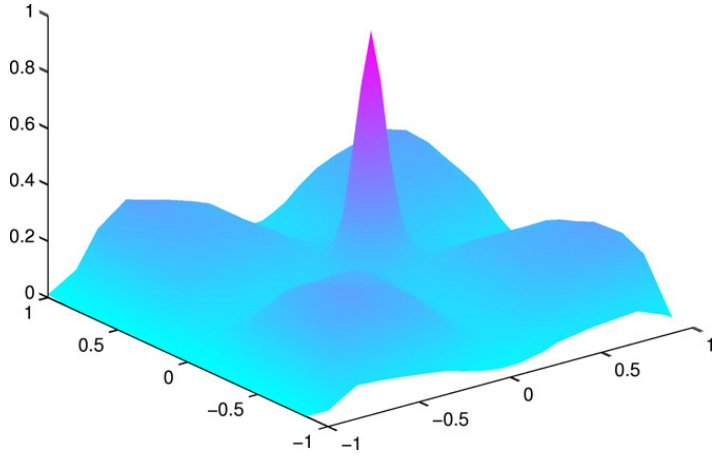

Fig. 8. Oscillatory behavior of a solution with hyperbolic i.c.

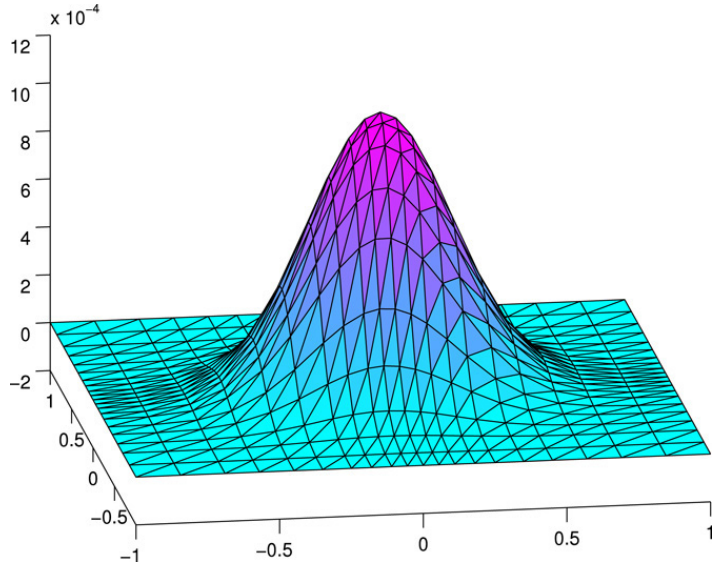

Fig. 9. Computed solution with Maxwellian initial condition (three projections have been performed).

supplies further improvement, basically, for Dirac and Maxwellian initial data. To calculate the L_1 and L_2 errors we use the vertex quadrature of the form:

$$\int_K g(x)\,\mathrm{d}x \approx \sum_{j=1}^{3} g(a_K^j)\frac{|K|}{3},$$

where a_K^j denotes the vertices of a triangle K, and $|K|$ denotes the area of K. Therefore

$$\|w\|_{L_1} \approx \frac{1}{3}\sum_K |K| \sum_{j=1}^{3} w(a_K^j), \quad \text{and} \quad \|w\|_{L_2} \approx \left(\frac{1}{3}\sum_K |K| \sum_{j=1}^{3} (w(a_K^j))^2\right)^{1/2}.$$

We also use the midpoint quadrature formula to get a weighed $\tilde{L}_2$ norm:

$$\|w\|_{\tilde{L}_2} \approx \left(\frac{1}{3}\sum_K |K| \sum_{1<=i<j<=3} (w(a_K^{ij})^2)\right)^{1/2},$$

where a_K^{ij} denotes the midpoint of the side connecting the vertices a_K^i and a_K^j. The errors in the $\tilde{L}_2$ norm are shown in Table 4.

Table 1
The L_∞ based norm for the errors between the "exact" and computed solutions

L_∞	Dirac	Hyperbolic	Maxwellian
CSD	47.6325	0.6878	0.6521
SSD	48.2734	0.6135	0.6521
CG	47.2871	0.6046	0.623

Table 2
The L_1 based norm for the errors between the "exact" and computed solutions

L_1	Dirac	Hyperbolic	Maxwellian
CSD	32.5463	0.1378	0.2912
SSD	33.4347	0.1535	0.2821
CG	36.1862	0.1546	0.3234

Table 3
The L_2 based norm for the errors between the "exact" and computed solutions

L_2	Dirac	Hyperbolic	Maxwellian
CSD	27.1325	0.1176	0.2031
SSD	27.1488	0.1135	0.2087
CG	31.9271	0.6036	0.2247

Table 4
The $\tilde{L}_2$ based norm for the errors between the "exact" and computed solutions

$\tilde{L}_2$	Dirac	Hyperbolic	Maxwellian
CSD	11.4339	0.1138	0.1342
SSD	11.2743	0.1155	0.1373
CG	12.7643	0.1264	0.1422

9. Summary and conclusions

We have given a formal derivation of the linear flatland transport equation and derived P_1, Fokker–Planck and Fermi approximations of a pencil beam model associated with this flatland model problem. We have considered four different deterministic algorithms for a pencil beam model based on the Fermi development. The algorithms are derived for a Standard Galerkin (SG)-, a Semi-Streamline Diffusion (SSD)-, a Characteristic Galerkin (CG)- and a Characteristic Streamline Diffusion (CSD)-method. Only the necessary qualitative behaviors of the schemes are quoted from the literature.

We carried out implementations to illustrate the applicability of the algorithms using different types of initial data approximating the Dirac δ function. To begin with, SSD and CSD are more stable and accurate than the SG and CG for all the three canonical forms of the initial data. As for the convergence: solutions with modified Dirac initial condition are suited in both CS and SSD. However, Maxwellian initial conditions produce accurate results in the CSD scheme, whereas the hyperbolic initial conditions produce more accurate results in the SSD scheme.

The oscillatory behavior, while considering non-smooth initial data, can be eliminated by modifying the L_2-projection. The formation of layers can be avoided taking small steps in the penetration variable. However, a better approach to deal with this phenomenon is through adaptive refinement. In order to keep this presentation simple, we did not address the adaptive algorithms here.

In general, for problems that are similar to our model problem (convection dominated convection–diffusion problems of degenerate type), streamline diffusion approaches such as SSD and CSD are more stable and accurate than the other related Galerkin schemes in the L_2-based norms.

Comments and future work

- A closely related study would be to consider the interesting question of seeing how the derivation in Section 2, and consequently the following sections, works looking at the special case of linearly anisotropic scattering. (This will require the full use of the spherical harmonic functions.) Specifically: how does the "flatland" differential scattering cross section relate to the original 3-D scattering cross section?
- The derivation in Section 2 shows that the "flatland" equation (2.8) is a "polar S_2" approximation to the x, y-geometry transport equation (2.4). It is most likely that the scaled flatland equation (2.6) will more accurately model diffusive problems in 3-D x, y-geometry (2.4). In other words, the flatland transport equation should be a good approximation to the 3-D transport equation for x, y-geometry diffusive problems.
- The approximation (2.6) raises an interesting question: what happens if, instead of an S_2 approximation to the μ-variable, we make an S_4 approximation? Then, we will get two equations of the form of Eq. (2.6), which will be coupled in the scattering term. This result should be more accurate than the Eq. (2.8). One may extend this idea to S_N in μ with $N > 4$. If there are transport problems in which the dependence of ψ on γ is more complicated than the dependence of ψ on μ, then the flatland approach could have practical merit. Otherwise a 2-D diffusion equation (with no angular variable) would be just as accurate.
- Intuitively, the diffusion coefficient in a general n-dimensional universe seems to be $\sim (1/n)\Sigma_{\text{tr}}$. Then, the customary "3" that we usually see occurs because we live in a 3-D universe. Planar-geometry problems have the factor 3 because these problems describe 3-D transport with 1-D symmetry. In a 2-D (flatland) universe, $n = 2$. In a 1-D universe (the rod model), $n = 1$.
- In the above derivations the scattering parameters, Σ_t, Σ_s, σ_t and σ_s, can be dependent on x and y.
- Finally a more realistic model should include energy dependence in the derivations described above and invoke numerical algorithms with adaptivity procedures.

Acknowledgments

The research of the first author is partially supported by the *Swedish Foundation for Strategic Research (SSF)* in the *Goteborg Mathematical Modeling Center (GMMC)*. We also thank Samir Naqos for making his codes available for this study.

References

[1] E.W. Larsen, A mathematical derivation of fermi theory and higher order corrections in electron dose calculations, Technical Report, Dept. Nucl. Eng. Univ of Michigan Ann Arbor, 1993.
[2] G.C. Pomraning, The transport theory of beams, Transport Theory Statist. Phys. 29 (2000) 1–41.
[3] C. Constantini, T.G. Kurtz, Diffusion approximation for transport processes with general reflection boundary conditions, Math. Models Methods Appl. Sci. 16 (2006) 717–762.
[4] M. Asadzadeh, On the stability of characteristic schemes for the Fermi equation, Appl. Comput. Math. 1 (2002) 158–174.
[5] M.H. Meylan, Wave scattering in the marginal ice zone, 2003. Preprint.
[6] G. Bal, V. Freilkher, G. Papanicolaou, L. Ryzhik, Wave transport along surfaces with random impedance, 2000. Preprint.
[7] A. Brahme, J. Nilsson, D. Belkic, Biologically optimized radiation therapy, Acta Oncol. 40 (2001) 725–734.
[8] D. Jette, Electron dose calculations using multiple-scattering theory. A Gaussian multiple scattering theory, J. Med. Phys. 15 (1988) 123–137.
[9] D. Jette, Electron beam dose calculations, in: Alfred R. Amith (Ed.), Radiation Therapy Physics, Springer-Verlag, Berlin, 1995, pp. 95–121; J. Med. Phys. 15 (1988) 123–137.
[10] D. Jette, Electron dose calculations using multiple-scattering theory. A new theory of multiple scattering, J. Med. Phys. 23 (1996) 459–476.
[11] D. Jette, Magnetic fields with photon beams: Dose calculation using electron multiple-scattering theory, Med. Phys. 27 (8) (2000) 1705–1716.
[12] D. Jette, Magnetic fields with photon beams: Monte Carlo calculations for a model magnetic field, Med. Phys. 27 (12) (2000) 2726–2738.
[13] D. Jette, Magnetic fields with photon beams: Use of circular current loops, Med. Phys. 28 (10) (2001) 2129–2138.
[14] J. Nilsson, B. Lind, A. Brahme, Radiation response of hyponic and generally heterogeneous tissues, Int. J. Radia. Biol. 78 (2002) 389–405.
[15] Marshak, Davis, See http://www.amazon.com/gp/product/3540239588/ref=wl_it_dp/105-9395120-8174854?ie=UTF8&coliid=IMHOM1QG87D08&colid=1D5DSYG8VP51I.
[16] E.E. Lewis, W.F. Miller Jr., Computational Methods of Neutron Transport, John Wiley & Sons, New York, 1984.
[17] Z. Luo, A. Brahme, High energy electron transport, Phys. Rev. B 46 (1992) 739–752.
[18] M. Olivares, W. Parker, W. Strydom, Electron beams: Physical and clinical aspects, in: E.B. Podgorsak (Ed.), Review of Radiation Oncology Physics: A Handbook for Teachers and Students, in: Rev. Educational Reports Series, International Atomic Energy Agency, 2004, pp. 225–248.
[19] M. Asadzadeh, The Fokker–Planck operator as an asymptotic limit in anisotropic media, Math. Comput. Modelling 35 (2002) 1119–1133.

[20] C. Börgers, E.W. Larsen, Asymptotic derivation of the Fermi pencil beam approximation, Nucl. Sci. Eng. 123 (16) (1996) 343–357.
[21] J. Coderre, Lecture notes in Principles of Radiation interactions, Department of Nuclear science and Engineering, MIT. Fall, 2004.
[22] E. Fermi, Cosmic ray theory, Rev. Modern Phys. 13 (1941) 240.
[23] E.W. Larsen, The nature of transport calculations in radiation oncology, Transport Theory Statist. Phys. 26 (1997) 739.
[24] G.C. Pomraning, The Fokker–Planck operator as an asymptotic limit, Math. Models Methods Appl. Sci. 2 (1992) 21–36.
[25] G.C. Pomraning, The screened rutherford pencil beam problem with heterogeneity's, Nucl. Sci. Eng. 136 (2000) 1–14.
[26] B. Su, G.C. Pomraning, A spatial and moment analysis of the monoenergetic pencil beam problem, Ann. Nucl. Energy 42 (1997) 1349–1371.
[27] J.A. Antolak, M.S. Bieda, K.R. Hogstrom, Monte Carlo method for commissioning electron beams, in: W. Schlegel, T. Bortfeld (Eds.), The Use of Computers in Radiation Therapy, Springer-Verlag, Berlin, 2000, pp. 449–451.
[28] C. Börgers, The radiation therapy planning problem, in: C. Börgers, F. Natterer (Eds.), Computational Radiology and Imaging: Therapy and Diagnostics (Proceedings of IMA Workshop, March 1997), in: IMA Volumes in Mathematics and its Applications, vol. 110, Springer-Verlag, 1999.
[29] C. Börgers, Complexity of Monte Carlo and deterministic dose calculation methods, Phys. Med. Biol. 43 (1998) 517–528.
[30] R.A. Boyd, K.R. Hogstrom, J.R. Antolak, A.S. Shiu, Measured data set for evaluating electron-beam dose algorithms, Med. Phys. 28 (2001) 950–958.
[31] R.A. Boyd, K.R. Hogstrom, A measured data set for evaluating electron beam dose algorithms, in: W. Schlegel, T. Bortfeld (Eds.), The Use of Computers in Radiation Therapy, Springer-Verlag, Berlin, 2000, pp. 231–233.
[32] K.R. Hogstrom, R.S. Steadham, P. Wong, A.S. Shiu, Monitor unit calculations for electron beams, in: J.P. Gibbons (Ed.), Monitor Unit Calculations for External Photon and Electron Beams, Advanced Medical Physics Publishing, Inc., Madison, WI, 2000, pp. 113–126.
[33] D.W.O. Rogers, A.F. Bielaje, Monte Carlo Techniques of Electron and Photon Transport for Radiation Dosimetry, in: Dosimetry of Ionizing Radiation, vol. III, 2002, pp. 2–19 (Chapter 5).
[34] C. Johnson, A new approach to algorithms for convection problems which are based on exacttransport + projection, Comput. Methods Appl. Mech. Engrg. 100 (1992) 45–62.
[35] M. Asadzadeh, A. Sopasakis, On fully discrete schemes for the Fermi pencil-beam equations, Comput. Methods Appl. Mech. Eng. 191 (2002) 4641–4659.
[36] M. Asadzadeh, A posteriori error estimates for the Fokker–Planck and Fermi pencil beam equations, Math. Models Methods Appl. Sci. 10 (2000) 737–769.
[37] M. Asadzadeh, Streamline diffusion methods for the Fermi and Fokker–Planck Equations, Transport Theory Statist. Phys. (1997) 319–340.
[38] F. Filbet, E. Sonnendrücker, Modelling and numerical simulations of space charged dominated beams in the paraxial approximation, Math. Models Methods Appl. Sci. 16 (2006) 763–791.
[39] T. Dupont, J. Hoffman, C. Johnson, R. Kirby, M. Larson, A. Logg, R.D. Scott, The FEniCS project, Chalmers Finite Element Center, Chalmers University of Technology. Preprint NO 2003:21, ISSN 1404-4382.
[40] S. Naqos, Numerical algorithms for electron beams, Master Thesis, Chalmers University of Technology, Department of Mathematics, 2005.